TRABAJO FIN DE GRADO

Grado en Biotecnología

Site-Directed Mutagenesis and Structural Modeling of the LiGAPDH–C5a Interface in Immune Evasion

Autor/es: **ZhongZe Hu**

Villaviciosa de Odón, *Junio 2026*

ÍNDICE

Abstract

Leptospirosis is a worldwide zoonotic disease caused by the bacteria *Leptospira interrogans* that escapes host immune defenses by multiple immune evasion strategies. One immune evasion strategy involves the glycolytic enzyme LiGAPDH, which acts as a moonlighting protein by binding to C5a of the complement system. The aim of this study was to explore the structural basis for the LiGAPDH-C5a interaction using site-directed mutagenesis (L34A, L98A, K193A) and then expressing and purifying the proteins. Six LiGAPDH mutants were made (three single site and three double site mutants), expressed, and subsequently purified using IMAC and SEC. The single site mutants maintained solubility and structural stability, while the double site mutants had a decrease in solubility which suggests that there was a cumulative destabilization due to both hydrophobic and electrostatic interactions. Docking simulations demonstrated limited variation in the selected docking scores among the wild-type and single mutants, supporting a qualitative model in which the interaction is broad and largely electrostatic in nature. Comparative analysis with other pathogenic species suggested that similar GAPDH–C5a interaction features are conserved, supporting electrostatic complementarity as a potential immune evasion mechanism. These data improve our understanding of immune evasion by bacteria and build a strong basis for targeted therapeutic strategies for leptospirosis.

Key words: *Leptospira interrogans*, GAPDH, C5a, immune evasion, docking, electrostatic complementarity, site-directed mutagenesis, complement system, structural biology, host-pathogen interaction

Introduction

1.1 The complement system

The complement system is a crucial component of the innate immune system, responsible for identifying and eliminating pathogens through a cascade involving over 30 glycoproteins, which are typically soluble in plasma or membrane-bound. This cascade is initiated via three activation pathways: classical, lectin, and alternative, each converging on the cleavage of complement protein C3 into C3a and C3b, using specific C3 convertases. The classical pathway, activated by antigen-antibody complexes, forms the C4b2a convertase with the involvement of C4 and C2. Similarly, the lectin pathway, initiated by mannose-binding lectin (MBL), which recognizes specific pathogen-associated sugar motifs, leads to the assembly of the C4b2a convertase. The alternative pathway is primed by the spontaneous hydrolysis of C3 into C3(H_2O), leading to the assembly of the C3bBb convertase, which in turn amplifies the pathway by generating more C3 convertase from native C3. Following this, C3b associates with the respective C3 convertases of its pathway to form C5 convertases—C4bC2aC3b in the lectin and classical pathways, and C3bBbC3b in the alternative pathway—leading to the cleavage of C5 into active fragments, C5b and C5a. The C5b fragment binds to the pathogen, initiating the formation of the membrane attack complex (MAC), which involves the sequential assembly of the C5b-C6-C7-C8-polyC9 complex, ultimately resulting in microbial lysis. [1,2]

Beyond direct pathogen elimination, the complement system has additional roles mediated by membrane-bound complement receptors such as CR1, CR3, and CR4, which are activated by complement fragments like C3b and iC3b. C3b and iC3b facilitate opsonization and enhance phagocytosis by neutrophils and macrophages. Additionally, subunits like C3a and C5a, although not directly involved in MAC synthesis, function as anaphylatoxins, mediating inflammatory processes by recruiting and activating immune cells. These subunits also increase vascular permeability and histamine release through interactions with specific G protein-coupled receptors like C3aR and C5aR1. [2]

Beyond its immunological roles, C5a activity has been implicated in pathological conditions like sepsis, where it contributes to immune dysfunction, organ failure, and apoptosis of specific

cell types such as thymocytes. Therefore, its regulation is critical to maintaining immune homeostasis and preventing tissue damage. Understanding C5a's diverse functions is essential for developing therapeutic interventions targeting complement-mediated diseases. [3,4]

However, many pathogens evade complement-mediated defenses by exploiting host regulatory mechanisms or through structural adaptations. Understanding these evasion strategies at the structural level is crucial for designing interventions that effectively target immune evasion mechanisms. [2]

1.2 Leptospirosis

1.2.1. General Description

Although the complement system plays an essential role in the clearance of pathogens, successful pathogens like *Leptospira interrogans* have developed highly sophisticated mechanisms to evade the effects of the complement, resulting in sustainable infection and systemic spread. [5]

Leptospirosis is a globally significant zoonotic disease that affects both urban and rural areas in developed and developing countries. It is caused by *Leptospira* bacteria and can be contracted through contact with contaminated water, soil, or the urine of infected animals. Leptospires enter the host through breaches in the skin or mucous membranes and spread through the bloodstream, colonizing various organs, including the liver, kidneys, and lungs. Symptoms range from mild flu-like symptoms to severe manifestations, such as Weil’s disease, including jaundice, kidney failure, and bleeding, or pulmonary hemorrhage, which can be fatal. Globally, leptospirosis causes over a million severe cases annually, with mortality rates reaching 10–15% in severe forms. [5,6]

The pathogenesis of *Leptospira* is still unclear, despite breakthroughs in molecular studies such as genome sequencing of *Leptospira* species. Treatment typically involves antibiotics like doxycycline or penicillin, although early diagnosis is critical for effective management. Prevention largely depends on improving sanitation and environmental management. As no universally effective vaccine currently exists, efforts are focused on developing polyvalent vaccines that address the diverse serovars of *Leptospira*. [5]

Molecularly, pathogenic *Leptospira spp.* lacks classical virulence factors, such as a type III secretion system, but rely on unique adaptations, including:

- Immune evasion: They recruit host complement regulators (e.g., factor H and C4b-binding protein) to their surface, avoiding complement-mediated lysis. They also degrade complement components like C3 and C5 through secreted proteases. [7]
- Adhesion and tissue colonization: Surface-exposed lipoproteins (e.g., LigB, Loa22) mediate adhesion to host matrix proteins including fibronectin, collagen, and laminin. These adhesins enable persistence in target tissues, particularly in immunoprivileged sites like the renal tubules. [7]
- Metabolic adaptations: Genes for vitamin B12 biosynthesis and catalase production enhance survival in nutrient-limited and oxidative environments, partly through the activity of catalase and superoxide dismutase, which degrade reactive oxygen species produced during host immune activation. [7]
- Environmental versatility: *Leptospira spp.* transition between free-living saprophytes and host-adapted pathogens. This dual lifestyle involves complex regulatory mechanisms, including two-component systems, sigma factors, and RNA-based thermosensors. [7]

The management of leptospirosis is based upon the phase and severity of disease. Antibiotics may reduce clinical deterioration or hospitalization during the early phase of illness, but in the severe or late stage, broad coverage antibiotics are preferred guided by renal safety. Given the immune-mediated damage during the late phase, the value of antibiotics is uncertain. Supportive therapies (i.e. corticosteroids, inhaled nitric oxide therapy, hemofiltration, plasma exchange) may be indicated to facilitate the management of complications. Overall, treatment of leptospirosis is complex due to lack of standardization and rigorously performed trials of severe disease and potential alternative treatment paradigms. [8]

1.2.2. LiGAPDH: Structure-Function Relationship in Immune Evasion

The glyceraldehyde-3-phosphate dehydrogenase (GAPDH) from *L. interrogans* (LiGAPDH), typically known as a glycolytic enzyme, exhibits "moonlighting" functions. Beyond its role in central metabolism, it also functions as an extracellular immune evasion factor. LiGAPDH can

interact with the anaphylatoxin C5a through weak, transient interactions. The crystal structure of LiGAPDH (PDB: 8OHA) reveals a homotetrameric holoenzyme with NAD^+ tightly bound to the N-terminal Rossmann fold domain (residues 1–152), which also includes the first catalytic residue, Cys152. The C-terminal catalytic domain (residues 153–335) harbors the remaining catalytic residues, His179 and Arg234. [9]

The immune evasion activity of LiGAPDH is mechanistically linked to three structural determinants [9]:

- Cys152-mediated covalent binding: Crosslinking studies suggest that LiGAPDH interacts transiently with C5a, and under certain conditions, Cys152 forms a stable disulfide bond that locks both proteins in a covalent complex.
- S-loop conformational flexibility: The dynamic S-loop (residues 180–207) may contribute to C5a binding by adopting different conformations that facilitate surface complementarity and interaction stability.
- Electrostatic complementarity: Electrostatic surface analyses suggest the presence of a positively charged region near the active site of LiGAPDH. This region may interact with a locally anionic patch on C5a, contributing to weak but specific binding.

These features collectively suggest that LiGAPDH's tetrameric architecture enhances binding avidity, enabling efficient sequestration of complement components at the pathogen-host interface. [9]

Building on this structural framework, LiGAPDH exerts its immune-evasive effects by directly binding and neutralizing C5a. Previous research by Dr. Cristina Vega's group has provided strong evidence of the affinity and specificity of this interaction. Bio-layer interferometry revealed binding of LiGAPDH to biotinylated C5a at 230 μM concentration, characterized by slow dissociation kinetics. Complementary, cross-linking studies with bis(maleimido)ethane identified covalent complexes between LiGAPDH and C5a. These interactions involved Cys27 in C5a and the highly reactive catalytic Cys152 in LiGAPDH, highlighting the role of thiol-mediated binding specificity. [9]

Moreover, structural modeling using cross-link-guided docking identified a detailed binding

interface, as shown in Figure 1 and the specific amino acids corresponding to these positions are listed in Annex 1. For C5a, residues surrounding Cys27 and regions within its two long helices were consistently involved. This interaction is further supported by electrostatic complementarity between the negatively charged face of C5a and the positively charged cavity of the LiGAPDH active site, as illustrated by the Adaptive Poisson-Boltzmann Solver (APBS-calculated) electrostatic surfaces shown in Figure 2. The flexible orientation of C5a's C-terminal helix further facilitated the interaction. [9]

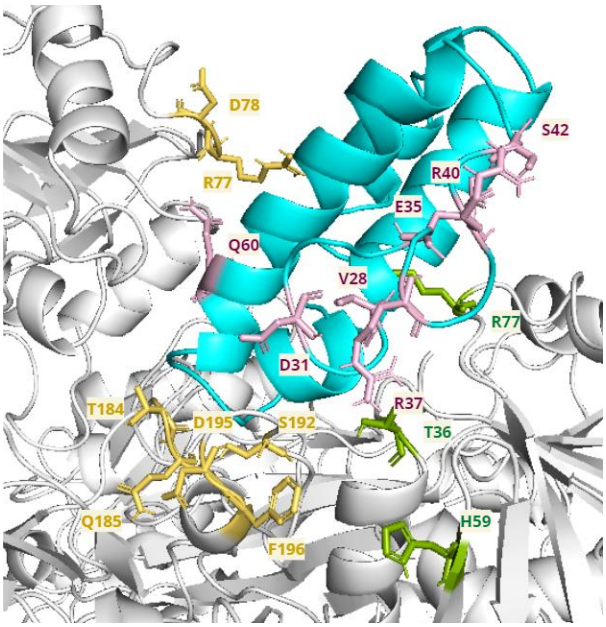

Figure 1: Structural interaction between LiGAPDH (PDB: 8OHA) and C5a (PDB: 1KJS). The LiGAPDH tetramer is shown in grey cartoon representation. Amino acid residues predicted to interact with C5a are highlighted in two different subunits: residues from one chain are shown in yellow, and residues from the other interacting chain are shown in splitpea (green). C5a is depicted in cyan, with its contact residues highlighted in light pink. The interaction model was obtained from ClusPro docking results, and the images were generated using PyMOL.

These findings highlight LiGAPDH as a pivotal virulence factor in *L. interrogans*, employing a precise and multifaceted mechanism to sequester C5a and inhibit complement activation, revealing new insights into bacterial immune evasion strategies. [9]

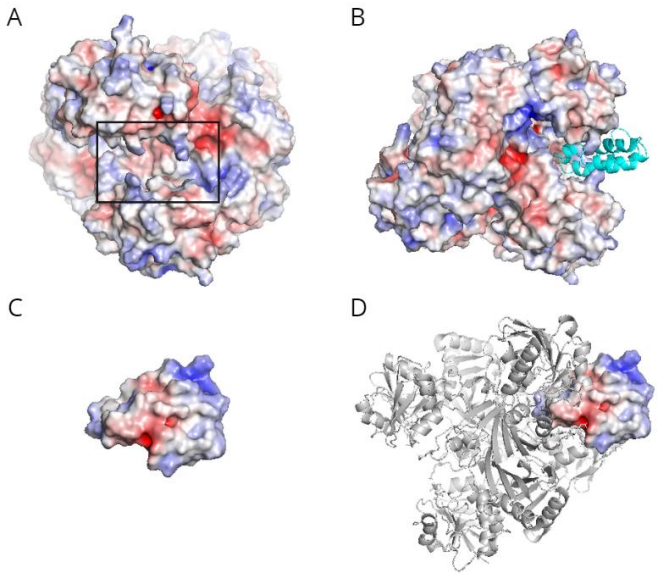

Figure 2: Molecular electrostatic potential maps of LiGAPDH (PDB: 8OHA) and C5a (PDB: 1KJS). (A) Electrostatic potential map of LiGAPDH, with the predicted binding interface highlighted by a black box. (B) Electrostatic potential map of LiGAPDH in combination with C5a shown as a cyan cartoon representation, illustrating their interaction. (C) Electrostatic potential map of C5a, displayed in the same orientation as in panel B. (D) Representation in the same orientation as panel B, where C5a is shown as an electrostatic potential map and LiGAPDH is depicted as a grey cartoon model. The interaction model was obtained from ClusPro docking results, and the images were generated using PyMOL.

Objective

General Objective:

To structurally and functionally characterize the immune evasion mechanisms mediated by the LiGAPDH protein of *L. interrogans*, focusing on its interaction with the complement component C5a, through an integrated approach combining experimental methods and computational simulations.

Specific Objectives:

1. To generate and validate six LiGAPDH mutant variants (three single mutants and three double mutants) using site-directed mutagenesis targeting residues L34, L98, and K193. Single mutants are (L34A, L98A, K193A), while double mutants combine two simultaneous substitutions (L34A/L98A, L34A/K193A, L98A/K193A) to investigate their impact on C5a interaction.
2. To express and purify mutant LiGAPDH proteins by immobilized metal affinity chromatography (IMAC) and size-exclusion chromatography (SEC), ensuring

structural integrity for downstream applications.

3. To perform molecular docking simulations between wild-type LiGAPDH and C5a using ClusPro, visualize the models in PyMOL, select the physiologically relevant docking conformation, and repeat the procedure for the monomutant variants.
4. To compare the docking results of wild-type and mutant LiGAPDH proteins with C5a by evaluating possible effects on the modeled interaction and interface architecture, to assess the impact of each individual mutation on the interaction.
5. To interpret the findings in the context of existing literature on GAPDH–C5a interactions, identifying key similarities or divergences to better understand bacterial immune evasion strategy.

Materials and Methods

2.1. Cloning Methods

2.1.1. Cloning Template, mutations and primers

To obtain the proteins of interest, the pETM-11 expression vector was used, which allows the production of recombinant proteins with an N-terminal His-Tag (a map of the vector is provided in Annex 2). The gene to be cloned was obtained from a template (DNA) previously verified by sequencing, and it was amplified by polymerase chain reaction (PCR) using specific primers.

To construct the recombinant plasmid, the *Escherichia coli* DH5α strain was used. Once the correct insertion of the gene into the vector was confirmed, the plasmid was introduced into the *Escherichia coli* Rosetta(DE3) pLysS strain.

To explore the functional importance of specific residues in LiGAPDH, a total of six site-directed mutants were generated by PCR: three single mutants (monomutants) and three double mutants. The details of each mutation, including the corresponding primer sets, are compiled in Table 1. Each pair of forward and reverse primers was designed to introduce or remove the intended amino acid change.

Table 1: Summary of site-directed mutations in LiGAPDH. Each entry is labeled in the format X##Y, where X is the original amino acid, ## is the position in the sequence, and Y is the new amino acid. For example, L34A means leucine (L) at position 34 is replaced by alanine (A).

Mutations
CVC0189: LiGAPDH-SM: L34A
CVC0190: LiGAPDH-SM: L98A
CVC0191: LiGAPDH-SM: K193A
CVC0192: LiGAPDH-DM: L98AK193A
CVC0193: LiGAPDH-DM: L34AK193A
CVC0194: LiGAPDH-DM: L34AL98A

2.1.2. Gene Amplification by PCR and Purification of DNA Fragments

PCR reactions were performed using Phusion® High-Fidelity DNA Polymerase (Thermo Scientific) in a final volume of 50 µL, containing 10 ng of template plasmid DNA (CVC0188, LiGAPDH wild type), 1x High-Fidelity (HF) or GC Buffer (tested independently), 0,2 mM dNTPs, 0,5 µM each of forward and reverse primers, 0.5 µL of DNA polymerase, and nuclease-free water to complete the volume. Thermal cycling conditions included an initial denaturation at 98 °C for 30 seconds; 30 cycles of denaturation at 98 °C for 10 seconds, annealing at 50.1 °C, 55 °C, or 59.9 °C for 20 seconds, and extension at 72 °C for 1.5 minutes; followed by a final extension at 72 °C for 5 minutes and a hold at 4 °C.

Amplification products were analyzed by electrophoresis on 1% (w/v) agarose gels prepared in 1× TAE buffer. For each sample, 10 µL of PCR product were mixed with 5 µL of 6× loading buffer and loaded into the gel (15 µL per well). A volume of 2.5 µL of DNA Ladder II (Thermo Scientific) was used as molecular weight marker. Gels were stained with GreenSafe Nucleic Acid Staining Solution (iNtRON Biotechnology) and visualized under UV illumination.

For determining optimal amplification conditions, reactions amplified were analyzed for the intensity of the specific band and the cleanliness of the lane during gel electrophoresis, indicating the absence of nonspecific banding and by-products. Ultimately, the buffer and annealing temperature combination with the greatest amplification efficiency and cleanest band profile were used in subsequent cloning strategies.

Because the initial electrophoresis results showed excessive noise in the agarose gel, PCR

samples were optimized with varying concentrations of DMSO (0%, 1%, and 3% v/v) to minimize oligonucleotide secondary structures. The optimized PCR products were then loaded onto a 1% (w/v) agarose gel for electrophoresis, allowing the separation and visualization of DNA fragments. The target DNA bands were carefully excised from the gel and purified using the NucleoSpin Gel and PCR Clean-up Kit (Macherey-Nagel), following the manufacturer's protocol to obtain high-purity DNA suitable for downstream mediation and conservation.

2.1.3. Ligation and transformation

After purification, the best PCR products from each reaction were subjected to a Kinase–Ligase–DpnI (KLD) reaction. Specifically, 1 µL of the purified PCR product was mixed with 5 µL of 2× KLD Buffer, 1 µL of 10× KLD Enzyme Mix (New England Biolabs), and 3 µL of nuclease-free water. The reaction was incubated at room temperature for 5 minutes.

For the transformation, 10 µL of the KLD reaction mixture was added to 100 µL of competent *E. coli* DH5α cells, followed by heat shock under standard conditions. The cells were then plated on Luria Bertani (LB) agar containing kanamycin (50 µg/mL) and 2% (w/v) glucose and incubated at 37 °C overnight.

After confirming that the plate was not contaminated, all colonies were picked and inoculated into 5 mL of LB medium supplemented with kanamycin to a final concentration of 50 µg/mL and 2% (w/v) glucose and grown at 37 °C with shaking at 200 rpm for further analysis.

2.1.4. DNA concentration measurement

DNA concentration was assessed utilizing ultraviolet light absorbance at 260nm, employing a NanoDrop microcuvette (Eppendorf µCuvette G1.0) connected to a spectrophotometer (Eppendorf BioSpectrometer). The ratio of absorbance employed was 260nm/280nm with the ideal range between 1.80 and 1.90. Plasmid solutions were adjusted (if necessary) with elution buffer to the measured DNA concentration to a final volume of 10 µL and 30 ng/µL DNA concentration. All samples were sequenced using the T7-F primer and data were analyzed for verification of presence and correctness of desired mutations.

2.2. Protein expression

2.2.1. Small-scale protein expression

Protein expression was performed using *E. coli* Rosetta (DE3) pLysS strain, which contains specific tRNAs not present in other *E. coli* strains. A 25 mL LB medium flask was inoculated with a bacterial colony or glycerol stock of the corresponding strain, supplemented with 50 μg/mL of kanamycin and 17 μg/mL of chloramphenicol. Cultures were incubated at 180 rpm and 37 °C.

After about 1.5 hours, when the optical density at 590 nm (OD590) reached 0.6–0.8, the cultures were acclimated at 20 °C for 1 hour. Protein expression was induced by adding 1 mM IPTG followed by incubation at 20 °C for 20 hours. Samples were collected at 3 hours, 20 hours, and from non-induced cultures for gel analysis.

To confirm protein expression, SDS-PAGE was performed. Cell lysates from each condition (non-induced, 3 hours post-induction, and 20 hours post-induction) were prepared by following the 2.3 Bacterial Lysis procedure (detailed steps are described in Section 2.3). For each sample, aliquots were taken both before and after centrifugation at 13,400 rpm for 5 minutes at 4 °C to verify that the expressed protein was present in the soluble fraction. This step ensures that the expressed protein is physiologically relevant and suitable for downstream purification.

The resulting supernatant (soluble fraction) and pre-centrifugation lysate were separately mixed with Laemmli sample buffer, boiled for 5 minutes at 95 °C, and loaded onto a 10% SDS-PAGE (v/v) gel. After electrophoresis, the gel was stained with Coomassie Brilliant Blue to visualize protein bands. [10]

2.2.2. Large-scale protein expression

For large-scale expression, small flasks (typically 100 mL, containing 25 mL LB medium) were inoculated with a colony or glycerol stock of the optimal strain, supplemented with antibiotics and 2% (w/v) glucose, and grown overnight at the optimal temperature to prepare the pre-inoculum. The next day, large flasks (typically 2 L, containing 500 mL LB/flask) were inoculated with the saturated pre-inoculum at a 1:100 (v/v) ratio. Cultures were grown under conditions similar to small expression, with IPTG added at the optimal concentration for

induction, followed by incubation for 20 hours at the optimal temperature.

Cells were harvested by centrifugation at 7,000 rpm for 20 minutes at 4 °C. Each pellet was weighed to record the biomass.

2.3. Protein purification: bacterial lysis, immobilized Metal Affinity Chromatography (IMAC) and Size-Exclusion Chromatography (SEC)

The purification process began by dissolving the cell pellet in 5 mL of buffer A (50 mM Tris-HCl, pH 8.0, 500 mM NaCl, 20 mM imidazole) per gram of cell mass, supplemented with 1 mM phenylmethylsulfonyl fluoride (PMSF). The cells were lysed by sonication using a cycle of 30 seconds on and 30 seconds off for a total of 15 minutes, ensuring the samples remained on ice to prevent overheating. After lysis, the insoluble fraction was separated from the soluble fraction by centrifugation at 7,000 rpm for 20 minutes at 4 °C. The soluble fraction was subsequently filtered using a 0.22 μm polyethersulfone (PES; Sartorius) membrane filter to remove any remaining particulate matter.

The generation of purified recombinant proteins was achieved utilizing immobilized metal affinity chromatography (IMAC). Recombinant proteins contained an N-terminal His-tag for specific binding to Ni^{2+} agarose resin. Initial small-scale purification experiments were performed using 200 μL of Ni^{2+} resin (HisPrep FF, Cytiva). The soluble fraction (input) was then added to 200 μL equilibrated Ni^{2+} resin with Buffer A contains 50 mM Tris-HCl (pH 8.0), 500 mM NaCl and 20 mM imidazole denoted as imidazole wash. After unbound proteins flowed through the column, the fractions were collected and two washes were performed with Buffer A and Buffer B contains 50 mM Tris-HCl (pH 8.0), 500 mM NaCl and 50 mM imidazole. The target protein was then eluted in a single step with 500 mM NaCl and 250 mM imidazole in Buffer C and designated as elution fractions. All fractions that contained input, flow through, washes, and elution were analyzed on SDS-PAGE (10% v/v) and were stained with Coomassie Brilliant Blue as a visual indicator for protein presence.

For the large-scale purification, the soluble fractions of each of the recombinant proteins were purified in the ÄKTA pure system (Cytiva) using a 1 mL HisTrap FF column. After the soluble fractions were added to the column and flow through fractions were collected, unbound protein

was washed out with Buffer A. After emptying the flow through fraction Buffer B, all histidine-rich proteins and metalloproteins could be washed out from the column. Subsequently, the target protein was eluted off the column in a single elution using Buffer C. All fractions that contained input, flow through, washes, and elutions were assayed by SDS-PAGE as previously described, to verify successful capture of the target protein and elution.

Following IMAC, proteins were polished and analyzed using Size-Exclusion Chromatography (SEC). Eluted proteins were first dialyzed overnight at 4 °C against SEC buffer (10 mM HEPES-NaOH, pH 7.4, 150 mM NaCl, 3.4 mM EDTA) to remove residual imidazole. Previously, samples from IMAC purification were concentrated using an Amicon Ultra concentrator (3 kDa; Millipore).

Proteins were then loaded onto a Superdex 200 Increase 10/300 GL column (Cytiva) connected to an ÄKTA pure system. Chromatographic parameters include SEC buffer as mobile phase (10 mM HEPES-NaOH (pH 7.4), 150 mM NaCl, 3.4 mM EDTA), flow rate of 0,5 mL/min and fraction size of 0.5 mL. Eluted fractions were analyzed via SDS-PAGE and stained with Coomassie Brilliant Blue, while protein concentrations were measured using UV absorption at 280 nm.

2.4. Molecular Simulation of the LiGAPDH-C5a Interaction in Mutants

To examine the structural ramifications of point mutations on the interaction of LiGAPDH with the complement chemotactic factor C5a, molecular docking simulations were performed with ClusPro and PyMOL. The crystal structure of wild-type LiGAPDH (PDB: 8OHA) and human C5a (PDB: 1KJS) served as the primary models for input in ClusPro. The crystal structure of wild-type LiGAPDH was uploaded to ClusPro 2.0 web server for protein–protein docking with C5a. Docking of wild-type LiGAPDH and C5a generated a set of candidate complexes for analysis. For the wild-type complex, the docking pose selected for further analysis was the one consistent with the interaction mode previously reported in the literature. The same structural criterion was then applied to identify the corresponding docking poses for the mutant variants, enabling a comparative analysis under a consistent binding mode. [9,11-17].

The point mutations L34A, L98A, and K193A were introduced into the wild-type LiGAPDH

structure using the Mutagenesis Wizard in PyMOL to generate structural representations. The substituted residues were highlighted in red, and the areas within a 5 Å radius surrounding each site of mutation were cleared to reduce any potential steric clashes. The new undisplayed mutated structures of LiGAPDH were saved in a PDB file format for later submission to ClusPro for docking experiments with C5a which was performed the same as it was done for the wild-type complex.

The docking outputs from the wild-type and mutant complex were compared in order to determine the change in binding affinity and other interaction parameters. The docking pose that was determined for the wild-type complex was carried forward as a reference point for comparing the subsequent impact of the point mutations in terms of structure and energetics on the wild-type binding mode of LiGAPDH with C5a.

Results and discussion

3.1. DNA cloning

PCR amplification of the double mutants, CVC0192, CVC0193, and CVC0194 (L98A/K193A, L34A/K193A, and L34A/L98A, respectively) displayed well-defined, specific bands in the agarose gel electrophoresis with no visible background or nonspecific amplification products (Figure 3). The absence of smearing or secondary bands indicates that the PCR was carried out under suitable conditions (i.e. GC buffer and range of annealing temperatures), and the amplification did not require any further tweaking with additives such as DMSO.

Assessing the clarity and intensity of the bands, we selected conditions for downstream processing, in samples we amplified accordingly: CVC0192 was amplified with GC buffer at 50.1°C and 55°C, CVC0193 with GC buffer at 50.1°C, and CVC0194 with GC buffer at 50.1°C and 55°C.

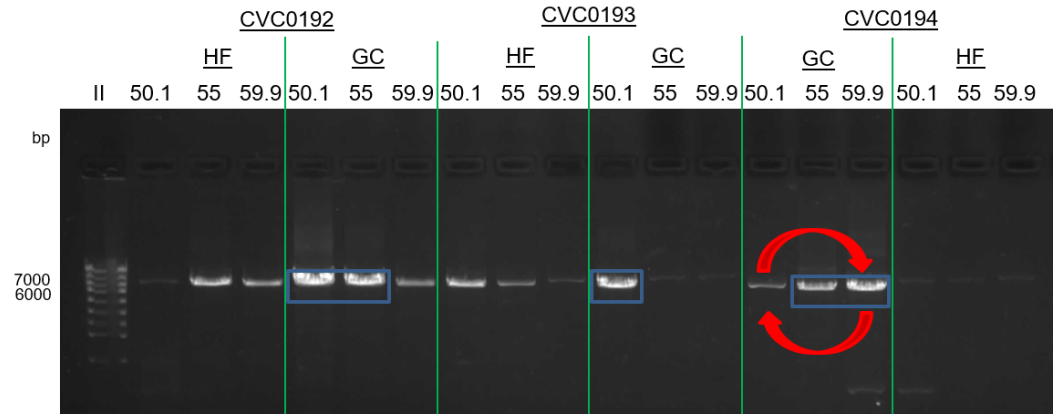

Figure 3: 1% (w/v) agarose gel electrophoresis of PCR products for CVC0192, CVC0193 and CVC0194 (double mutants of LiGAPDH: L98A/K193A, L34A/K193A and L34A/L98A) PCR was performed using HF and GC buffers at three separate annealing temperatures of 50.1 °C, 55 °C and 59.9 °C. Blue boxes indicate the bands that were chosen for purification. The results of the GC buffer condition for CVC0194 for the 50.1 °C and 59.9 °C were swapped during sample loading due to a technical error.

In the cloning assays of the three monomutants (CVC0189, CVC0190, and CVC0191), the agarose gel showed multiple nonspecific bands (Figure 4), indicative of a significant amount of background noise in the PCR reactions. This was possibly due to a high propensity for stable, secondary structure formation in the template, or nonspecific annealing of primers, both of which can affect amplification specificity.

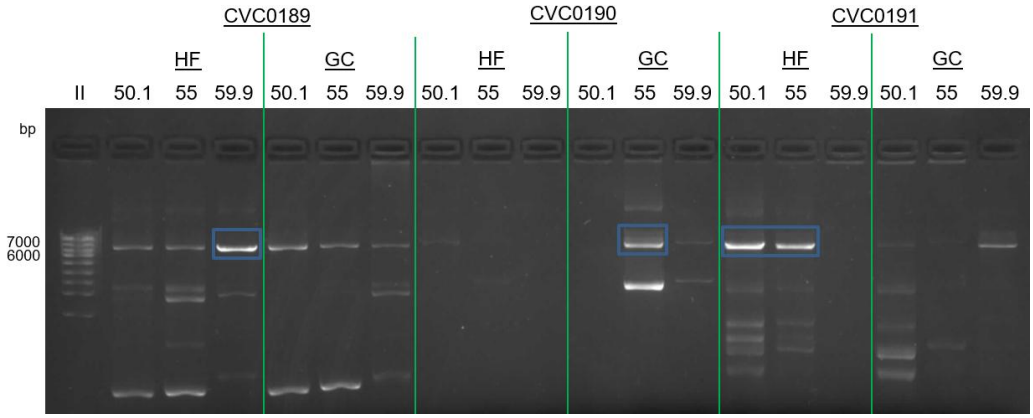

Figure 4: 1% (w/v) agarose gel electrophoresis of PCR products for CVC0189, CVC0190, and CVC0191 (single mutants of LiGAPDH: L34A, L98A, and K193A, respectively). All samples were amplified at three different annealing temperatures (50.1 °C, 55 °C, and 59.9 °C) using HF and GC buffers.

However, amplification of the double mutants, (CVC0192, CVC0193, and CVC0194) yielded clearer and more specific band patterns, with little to no visible background and no missing bands. These observations suggest that not only buffer choice and annealing temperature, but also likely other intrinsic factors related to sequences, such as local GC content, secondary

structure propensity, or context-dependent primer binding, could have some significant effect on amplification outcomes and should be scrutinized when designing experiments.

To improve the amplification specificity observed in the monomutant constructs, the products of PCR reactions were optimized by incorporating DMSO at concentrations of 0%, 1%, and 3% (v/v) (Figure 5). It was observed that for CVC0189 (L34A), the addition of DMSO reduced background noise, but not significantly regardless of the HF or GC buffer conditions. Again, for CVC0191 (K193A), using DMSO the HF buffer didn't significantly decrease nonspecific amplification. The remaining conditions showed only modest improvements in band specificity. In the CVC0190 (L98A), the GC buffer at 55 °C resulted in a clean and well-defined band.

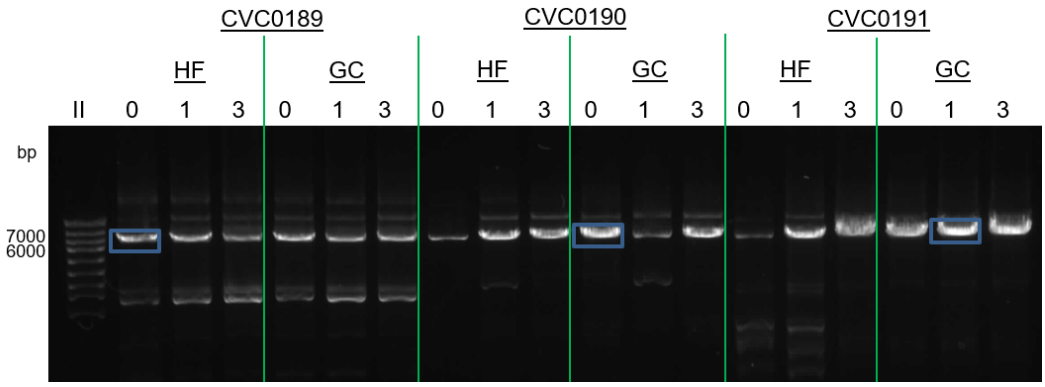

Figure 5: 1% (w/v) agarose gel electrophoresis of PCR products for CVC0189, CVC0190, and CVC0191 (single mutants of LiGAPDH) following DMSO optimization. Each sample was amplified using HF or GC buffer with 0%, 1%, or 3% (v/v) DMSO. The bands selected for further analysis are highlighted with blue boxes.

Based on these results, the following conditions were selected for further quantification and analysis: CVC0189 (L34A) amplified with HF buffer at 59.9 °C, CVC0190 (L98A) with GC buffer at 55 °C, and CVC0191 (K193A) with GC buffer, 50.1 ºC and 1% v/v DMSO.

Following gel extraction under previously optimized PCR conditions, concentrations and purity (A260/A280) for DNA were taken for each of the six samples selected. For the monomutants, the yields were as follows: CVC0189 (L34A) amplified in HF buffer at 59.9 °C had yield at 74.8 ng/µL, A260/A280 ratio of 1.77 (total 1.12 µg in 15 µL); CVC0190 (L98A), amplified in GC buffer at 55 °C had yield of 103.7 ng/µL, A260/A280 of 1.80 (1.55 µg total); and CVC0191 (K193A) was amplified in GC buffer, 1% (v/v) DMSO at 50.1 °C had yield of 136.8 ng/µL, A260/A280 of 1.88 (2.05 µg total).

For the double mutants, CVC0192 (L98A/K193A) amplified in GC buffer at 55 °C had yield of 124.4 ng/µL, purity ratio of 1.80 (1.86 µg total); CVC0193 (L34A/K193A) showed a somewhat lower yield at 48.9 ng/µL, A260/A280 ratio of 1.75 (0.73 µg total). Finally, CVC0194 (L34A/L98A) amplified at 50.1 °C also, revealed a yield of 81.8 ng/µL, A260/A280 of 1.86 (1.22 µg total).

All samples showed A260/A280 ratios in the acceptable purity range of 1.75 and 1.90. Values at 1.80 are generally considered optimal for plasmid DNA, as these values indicate low protein contamination and high quality for downstream purposes.

3.2 Expression

To assess the expression and solubility of LiGAPDH mutants, constructs CVC0189 to CVC0194 were expressed in *E. coli* Rosetta (DE3) pLysS cells carrying the pETM-11 plasmid and analyzed by SDS-PAGE (10% v/v) (Figures 6A, B, C). Gels were stained with Coomassie Brilliant Blue, and each gel included molecular weight markers (MW), non-induced (NI) controls, total protein extracts (T), and soluble protein fractions (Sol), both extracts collected at 3 h and 20 h post-induction. Relative to the total and soluble extracts from each time point, the protein band corresponding to the LiGAPDH monomer (~37 kDa) was clearly seen in all samples. There were also faint bands in the NI lanes for all mutants. These bands suggest LiGAPDH was being expressed in the absence of IPTG, likely consistent with leaky basal expression typical of T7-based expression systems. In all cases, the band intensity markedly stronger post-induction, especially at the 20 h time point, indicating effective time-dependent expression of all constructs. [18]

Comparing the fractions total (T) and soluble (Sol), the overall solubility differences in solubility between monomutants and double mutants could be observed. Each of the monomutants (CVC0189, CVC0190, and CVC0191) showed the soluble fractions bands of similar intensity to the total fractions, suggesting that these single-point mutations did not affect protein folding or solubility. These proteins were properly expressed and stayed soluble, making them ready candidates for downstream purification and analysis.

A contrasting trend was established for the double mutants (CVC0192, CVC0193, and

CVC0194) as they were all characterized by substantially reduced solubility even with highly expressed total yield across all mutants. There was a strong total extract band established at 20 h for each mutant; however, the soluble fractions were much weaker (Figures 6B-6C). This indicated that much of the desired expressed protein was insoluble, and likely in inclusion bodies. This pattern was consistent across all double mutants.

In terms of understanding the loss of solubility, an exploration of the structural context of the mutated residues could provide insight. Leucine-34 (L34) and Leucine-98 (L98) are likely buried hydrophobic residues that help stabilize the core of the protein. Mutation to alanine (L34A or L98A) represents a reduction in side-chain volume that disrupts hydrophobic packing which marginally destabilizes the protein but is ultimately likely tolerated as each residue is individually mutated to alanine. In contrast, both mutations at once (e.g., CVC0194: L34A/L98A) produces cumulative destabilization to the core, ultimately creating cavities or mis-folded intermediate forms. Similarly, Lysine-193 (K193) represents a positively charged residue that would likely be surface exposed and that possibly help overall solubility of protein locally through solvent interactions or contribute to local structural stabilization via ionic interactions. The mutation to alanine (K193A) removes a favorable electrostatic contribution that could promote aggregation. When comparing the systematic destabilization of the L34, L98 combined with K193, and combined on a structural level causing three inevitable destabilizing influences on structural stability on the core (loss of buried hydrophobic stability at the core), disruption of local folding (loss of K193 contribution to structured stability), and greatest impact on protein solubility (loss of surface charge). This combined event would likely increase the likelihood for the protein to misfold and aggregate during expression resulting in a lower soluble yield. In contrast, single mutations are more likely allowed for the perturbations to not be as limiting as aggregate perturbation states. [19,20]

Thus, in terms of suitability for purification and downstream functional analyses, only the monomutants were selected for further large-scale studies, as they exhibited adequate structural stability and solubility under native conditions. Although preliminary small-scale purification trials were conducted for the double mutants, their markedly reduced solubility represented a

major limitation. Consequently, these variants were not pursued further for large-scale purification or subsequent functional and structural characterization, including assays related to immune evasion.

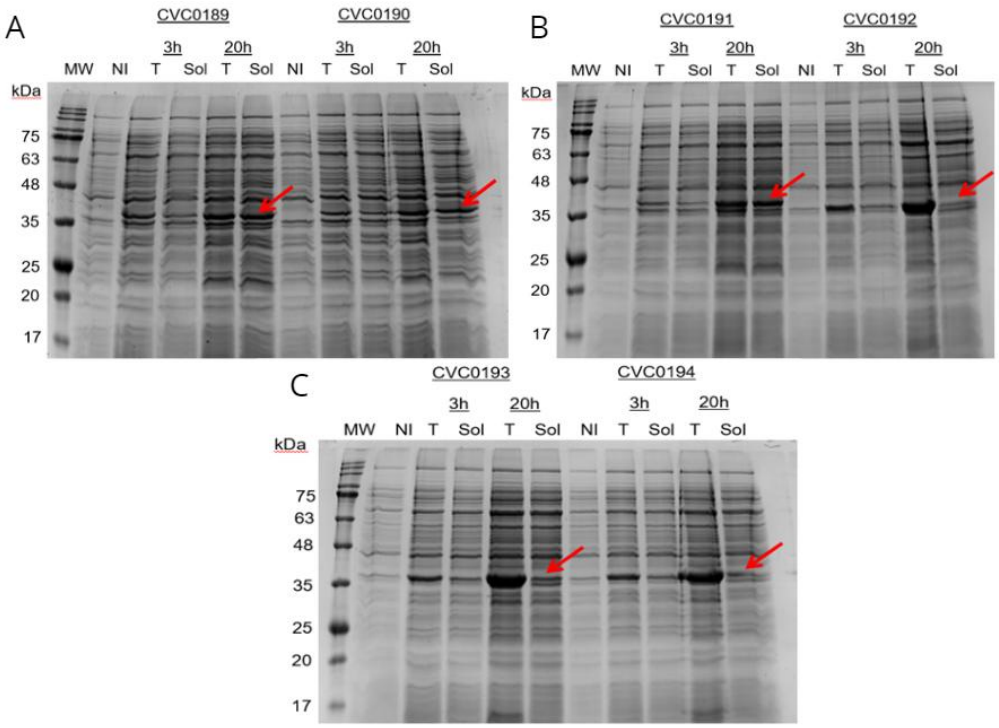

Figure 6. SDS-PAGE (10% v/v) analysis of the expression of LiGAPDH mutant variants. Samples were collected at 3 h and 20 h post-induction and stained with Coomassie Brilliant Blue. Lane labels: MW – molecular weight marker; NI – non-induced control; T – total protein extract; Sol – soluble fraction. (A) Expression of CVC0189 (L34A) and CVC0190 (L98A). (B) Expression of CVC0191 (K193A) and CVC0192 (L98A/K193A). (C) Expression of CVC0193 (L34A/K193A) and CVC0194 (L34A/L98A). Red arrows indicate the expected position of the LiGAPDH mutant bands in the soluble fractions.

3.3 Protein purification

3.3.1 Purification - IMAC Ni^{2+} resin

All six LiGAPDH mutants were purified on a small scale (200 µL Ni^{2+} resin) under native conditions. The SDS-PAGE (10% v/v) gels identified by Figure 7A-C were used to track the purification procedure for each protein at five main time points for tracking purities: Input, Flow-through, Wash1, Wash2, and Elution.

The input samples for each construct show a dominant band at the expected molecular weight (~37 kDa), indicating that LiGAPDH is present in the soluble extract before purification; the elution samples show presence of LiGAPDH with a band observable in the same region as

observed in the input samples which indicates that His-tagged LiGAPDH was successfully captured via immobilised metal affinity chromatography (IMAC).

The elution samples for the monomutants were very strong for LiGAPDH (CVC0189, CVC0190 and CVC0191), indicating a great recovery of soluble protein. The elution samples for the double mutants (CVC0192, CVC0193 and CVC0194) show only faint bands for LiGAPDH; as we have observed before, representations of low solubility observed in the expression analysis above.

Collectively, these observations show that double mutations are negatively impacting protein recovery, which is due to lower solubility observed as increased aggregation. Therefore, only the monomutant constructs (CVC0189, CVC0190, and CVC0191) were taken forward to large scale purification and biochemical characterization; whilst the double mutants are unsuitable for any downstream analyses, due to low yields.

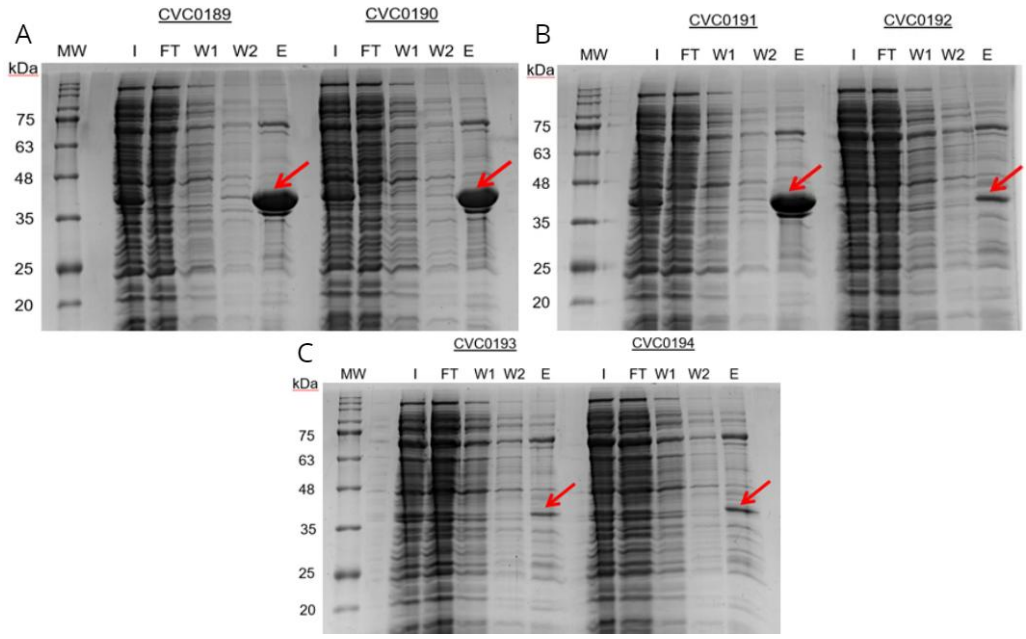

Figure 7. SDS-PAGE (10% v/v) analysis of IMAC purification of LiGAPDH mutant variants using 200 µL of Ni^{2+} resin. Lane labels: MW – molecular weight marker; I – input (total protein before binding); FW – flow-through (unbound fraction); W1, W2 – sequential wash fractions; E – elution (purified protein). All samples were stained with Coomassie Brilliant Blue. (A) Purification of CVC0189 (L34A) and CVC0190 (L98A). (B) Purification of CVC0191 (K193A) and CVC0192 (L98A/K193A). (C) Purification of CVC0193 (L34A/K193A) and CVC0194 (L34A/L98A). Red arrows indicate the expected position of the LiGAPDH bands.

3.3.2 Purification – IMAC HisTrap FF 1 ml

The large-scale purification of the CVC0189 (L34A) mutant using a 1 mL HisTrap FF column yielded multiple elution fractions (E13–E18), in which a clear LiGAPDH band can be observed by SDS-PAGE (Figure 8A). Among them, fractions E15 and E16 displayed the most intense bands at the expected molecular weight, indicating a higher concentration of the target protein in these samples. However, multiple additional bands of background were also present across several lanes, suggesting co-purification of non-specific proteins and pointing to a need for further purification steps. In addition to SDS-PAGE analysis, fast protein liquid chromatography (FPLC) was used to further evaluate the protein content. Fraction E16 corresponded to a prominent chromatographic peak eluting at approximately 45.42 mL, reflecting the presence of UV-absorbing species—presumably the His-tagged LiGAPDH protein (Figure 8B).

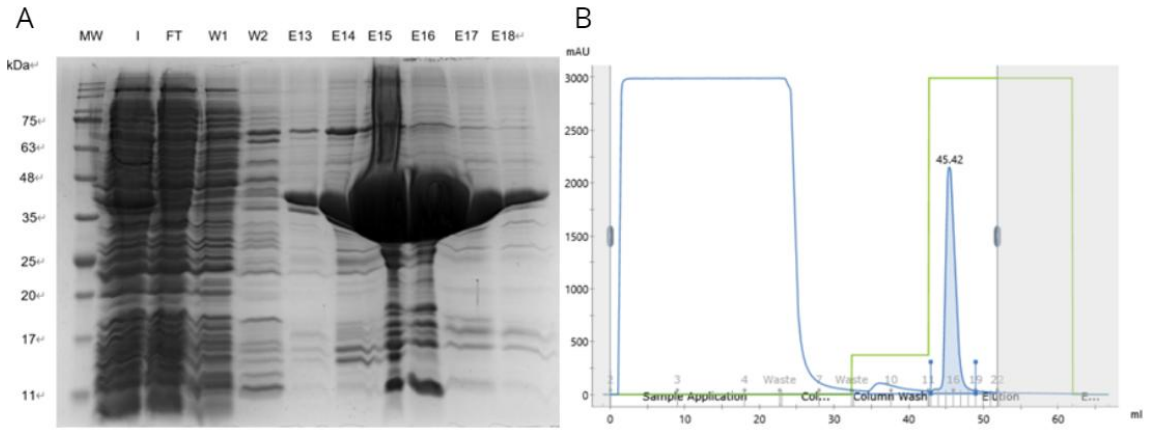

Figure 8. Large-scale IMAC purification of CVC0189 (L34A) using a 1 mL HisTrap FF column on an ÄKTA system. (A) SDS-PAGE (10% v/v) analysis of the purification. Lanes: MW – molecular weight marker; I – input (total protein before loading); FT – flow-through; W1, W2 – first and second wash fractions; E13–E18 – sequential elution fractions. The gel was stained with Coomassie Brilliant Blue. (B) Corresponding chromatogram of the purification process.

SDS-PAGE analysis of the IMAC purification of CVC0190 (Figure 9A) revealed the presence of LiGAPDH in fractions E13–E18, with the most prominent bands in E14 and E15. As with the previous construct, background bands were visible, indicating partial purity. FPLC chromatogram analysis (Figure 9B) showed a peak corresponding to fraction E16, eluting at approximately 45.57 mL, confirming the presence of protein in line with the gel results.

Although the highest gel intensity was observed in E14–E15, the chromatographic peak in E16 suggests some overlap in elution. Overall, CVC0190 was successfully recovered, though additional polishing steps may be needed. Due to time limitations, the purification of CVC0191 was not carried out.

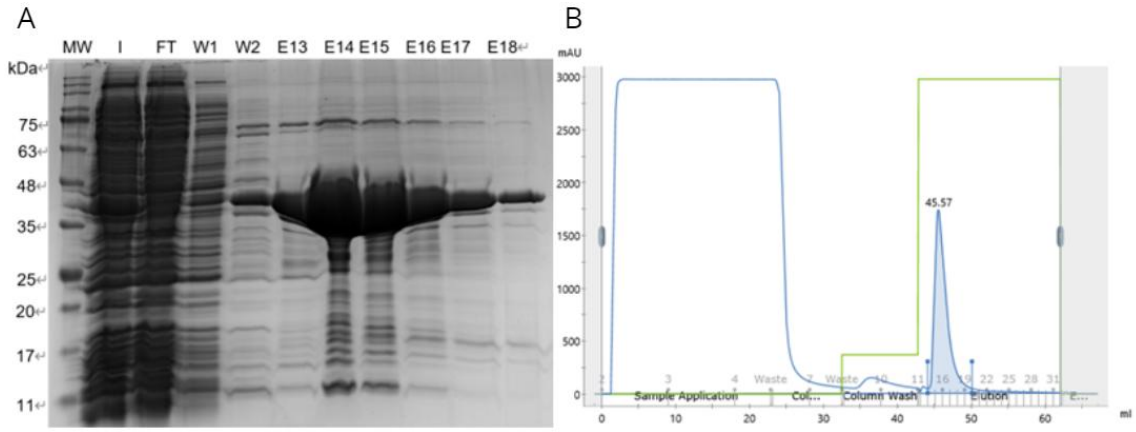

Figure 9. Large-scale IMAC purification of CVC0190 (L98A) using a 1 mL HisTrap FF column on an ÄKTA system. (A) SDS-PAGE (10% v/v) analysis of the purification; lane labels are as described in Figure 8. (B) Corresponding chromatogram of the purification process.

3.3.3 Purification – SEC

Following IMAC purification, the CVC0189 (L34A) mutant was further purified by size-exclusion chromatography (SEC) using a Superdex 200 Increase 10/300 GL column. As shown in Figure 10A, SDS-PAGE analysis of the SEC fractions revealed a strong LiGAPDH band in the input (I) and in elution fractions E15–E19, with markedly reduced background compared to the IMAC gel. Fractions E16 and E17, highlighted in blue, were selected for storage due to their high purity and protein concentration. The corresponding FPLC chromatogram showed a peak in fraction E17 with a maximum absorbance at 13.33 mL (Figure 10B). The final yield of purified protein was 3.2 mg of LiGAPDH L34A per liter of culture.

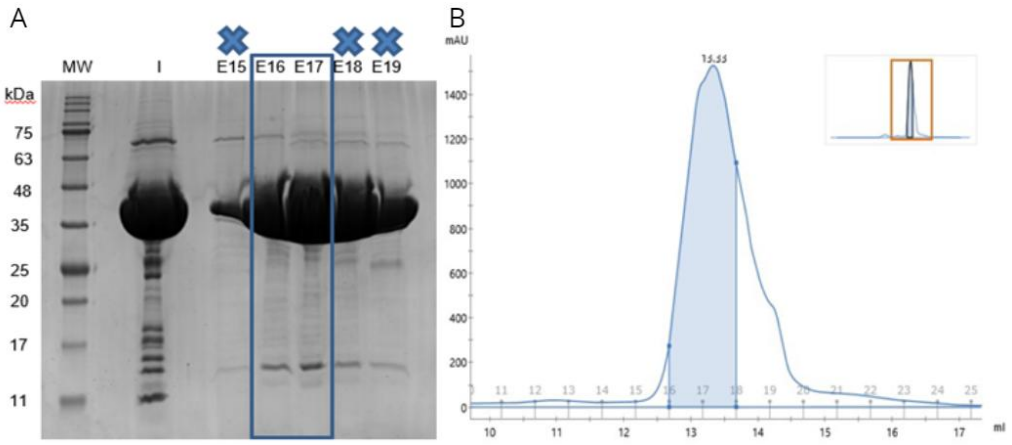

Figure 10. Analysis of CVC0189 (L34A) purification by size-exclusion chromatography (SEC) using a Superdex 200 Increase 10/300 GL column. (A) SDS-PAGE (10% v/v) analysis of elution fractions. Lane labels: MW – molecular weight marker; I – input; E15–E19 – eluted fractions. (B) Corresponding SEC chromatogram showing UV absorbance at 280 nm.

CVC0190 (L98A) continued to be purified by SEC on a Superdex 200 Increase 10/300 GL column. In Figure 11A, the SDS-PAGE gel demonstrated some distinct LiGAPDH bands appearing as being in fractions E16-E20. Fractions E17 and E18 were most intense and had the best purity. Background noise was much improved compared to previous purification steps. Both practical fractions E17 and E18, which are both labelled in blue in the SDS-PAGE gel, were selected for later use and to be stored. The elution profile obtained from FPLC demonstrated a similar output to the SDS-PAGE (Figure 11B). The peak in fraction E18 had a maximum absorbance at 13.27 mL that was consistent with the output noticed in SDS-PAGE. The final protein yield was 5.6 mg of LiGAPDH L98A per liter of culture.

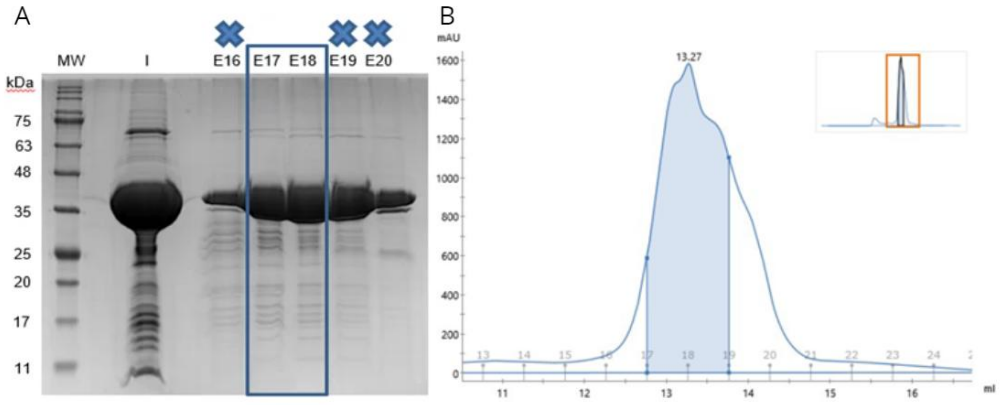

Figure 11. Analysis of CVC0190 (L98A) purification by size-exclusion chromatography (SEC) using a Superdex 200 Increase 10/300 GL column. (A) SDS-PAGE (10% v/v) analysis of elution fractions. Lane labels: MW – molecular weight marker; I – input; E16–E20 – eluted fractions. (B) Corresponding SEC chromatogram showing UV absorbance at 280 nm.

3.4 Effect of Selected Single-Point Mutations on the Modeled Interaction Between LiGAPDH and C5a

After performing protein-protein docking analysis, 10 poses were obtained and the most likely docking pose was identified for wild-type LiGAPDH and monomutants. For the wild-type complex, the docking pose selected for further analysis was the one consistent with the interaction mode previously reported in the literature. The corresponding poses for the three single-point mutants were then selected using the same structural criterion, allowing comparison under a common binding mode. Table 2 summarizes the ClusPro docking scores obtained for the selected wild-type and mutant complexes. [12-16,17]

Table 2: ClusPro docking scores for the selected LiGAPDH wild-type and single-point mutant complexes with C5a. Values are shown in arbitrary units.

Mutation	Lowest docking score
LiGAPDH wild-type	-616.9
CVC0189_L34A	-623.8
CVC0190_L98A	-602.0
CVC0191_K193A	-631.6

Overall, the selected single-point mutants showed docking scores within a similar range to that of the wild-type complex. However, these values should be interpreted cautiously, as docking scores obtained from rigid-body computational approaches are only approximate estimates of interaction energies rather than direct quantitative measures of binding affinity. In ClusPro, docking solutions are evaluated mainly through clustering of low-energy conformations rather than by the absolute value of a single score. Therefore, the limited score differences observed here are better interpreted qualitatively than quantitatively and do not support strong conclusions regarding the energetic contribution of individual residues. [12,14,15,17]

The data derived from the docking simulations suggest that the selected single-point mutations at residues L34, L98, and K193 did not produce major changes in the modeled LiGAPDH–C5a interaction under the selected binding mode. In this context, these results suggest that these residues may not individually make a dominant contribution to the overall interaction. This is further illustrated in the docking visualization images provided in Annex 3 (A-D).

The interaction interface between C5a and LiGAPDH is located within a highly charged environment, supporting an important role for electrostatic complementarity. However, the replacement of the positively charged lysine at position 193 with a neutral alanine in the CVC0191 (K193A) mutant resulted in little change in the docking score, suggesting that K193 alone may not be a dominant contributor to the electrostatic stabilization of the modeled complex. This observation is further supported by the electrostatic surface analysis shown in Figure 12, where two minor alterations in the electrostatic potential can be observed in the mutated region (highlighted with yellow boxes) compared to the wild-type (Figure 12A). Though these changes are observable within a small region, in terms of the larger electrostatics of the cavity, the positively charged cavity appears to remain intact, consistent with the docking analysis. [9]

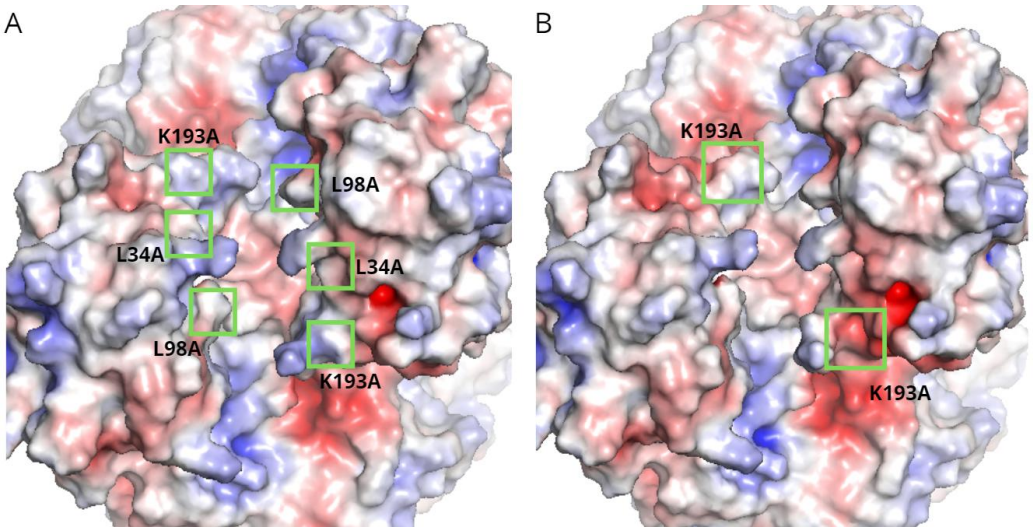

Figure 12: Electrostatic potential surface representations of LiGAPDH wild-type (WT) and the K193A mutant, generated in PyMOL. The LiGAPDH structure (PDB: 8OHA) was used as a template, and the K193A variant was constructed in silico using the PyMOL mutagenesis tool. (A) WT. (B) K193A. Electrostatic maps of L34A and L98A are shown in Annex 4A and 4B.

Similarly, L34A and L98A mutations (Annex 4) did not produce significant differences in the docking energy score, nor did they induce notable changes in the electrostatic surface, indicating that these residues do not play a dominant role in defining the interaction interface.

Collectively these results suggest that the selected single point mutations included limited effects on the modeled interaction and that the interface may be defined by the combined contribution of multiple residues rather than by direct effects of individual key residues.

Although these results should not be interpreted as quantitative measurements of binding affinity, they are consistent with the idea that the LiGAPDH–C5a interface is broad, tolerant to point substitutions, and largely electrostatic in nature. Additional mutagenesis and experimental validation of wild-type and mutant LiGAPDH in complex with C5a will be necessary to determine the actual contribution of these residues to the physical interaction. [9]

When compared with similar studies in other pathogens, this seems consistent. In *Streptococcus pyogenes*, surface-exposed GAPDH was shown to bind C5a and contribute to immune evasion by sequestering C5a and inhibiting neutrophil recruitment. Although its contribution to function has been documented, the interaction has not related to specific amino acids as there are no mutations that have been identified, although it has been suggested that a positively charged patch in the N-terminal region, near the NAD^+-binding site contributes to the interaction. Similarly, *Atopobium vaginae* GAPDH was shown to bind C5a through the same positive charge, surface-exposed, N-terminal structure, as indicated by biochemical studies and inhibition of chemotaxis. [21,22]

In *Clostridium perfringens*, the binding of GAPDH to C5a was less effective, resulting in only partial inhibition of neutrophil migration. Although the binding interface to C5a still has not been structurally defined, these studies seem to suggest that the binding is likely using the same conserved surface of electrostatic interaction, not with specific residues that are irreplaceable. This supports the interpretation in *L. interrogans* that even mutation of the selected positively charged or hydrophobic residue should maintain the modeled interaction, suggesting that there is redundancy and cooperativity in the binding surface. [23]

Furthermore, the insignificance of affinity and reversible character of these associations may provide an evolutionary benefit for bacteria, as it allows for short-term masking of C5a without developing stable and irreversible interactions that may heighten bacterial risk of immune recognition or treatment response. In addition, GAPDH alone appears to be adequate to sequester C5a and reduce complement activation and postpone neutrophil recruitment, which suggests that this mechanism represents a general immune evasion strategy in very diverse bacterial species. [9,22]

Collectively these results indicate that several pathogenic bacteria have evolved the ability to redeploy cytosolic GAPDH proteins to the surface of the bacteria as a virulence factor that is capable of opportunistically targeting host C5a. This mechanism allows bacteria to interfere with host complement system activity via C5a masking or sequestration, which dampens neutrophil recruitment and delays activation of an immune response. Several studies, including binding and cross-linking analyses of *S. pyogenes* as well as chemotaxis inhibition assays of *A. vaginae* and *C. perfringens*, demonstrate that GAPDH from these bacteria influence complement activity via targeting C5a and dampening host immune activity. [9,21-23]

The docking results shown in this study, in combination with cross-linking studies in *L. interrogans*, add additional structural insight into how this interaction might occur at the molecular level and support the importance of a wide electrostatically favored surface as opposed to a narrowly specific binding pocket. These docking results support our hypotheses that GAPDH–C5a interactions are flexible and robust, able to tolerate amino-acid sequence variations while relying on the general electrostatic nature of the interface as the main driver of the interaction.

These results indicate how diverse bacterial pathogens may evolve common molecular mechanisms to interfere with host immunity. While also highlighting that binding efficiency may differ, evidence suggests that the GAPDH–C5a interaction itself is a conserved and flexible virulence mechanism that deserves further examination especially regarding therapeutic development.

3.5 ODS thinking

This study underscores the importance of bioinformatics and biochemical approaches for identifying key residues involved in host–pathogen interactions, involved in the interaction with the pathogen, specifically *L. interrogans*. This information could inform future rational designs of vaccines and therapies that are targeted toward bacterial infectious disease. Additionally, this work aligns with Sustainable Development Goal 3 (SDG 3): Good Health and Well-being, contributing to broader efforts aimed at combating infectious diseases with significant public health impact, such as leptospirosis.

Conclusion

Generation, Expression and Structural Analysis of Mutants: Through site-directed mutagenesis, we generated six LiGAPDH mutants (three single mutans and three double mutants). Single mutants required PCR optimization with 1-3% (v/v) DMSO to reduce background amplification, while double mutants showed cleaner amplification profiles, potentially due to reduced secondary structures (Objective 1 achieved). Protein expression revealed striking differences: single mutants remained soluble (3.2-5.6 mg/L yield after IMAC/SEC purification), while double mutants showed significantly reduced solubility. This demonstrates that combined mutations cumulatively destabilize protein structure, particularly affecting hydrophobic core residues (L34, L98) and surface electrostatic interactions (K193), fulfilling Objective 2 while highlighting the critical balance between structural stability and enzymatic function.

LiGAPDH-C5a Interaction Analyses: Molecular docking analyses showed limited variation in the selected docking scores of the LiGAPDH–C5a complexes upon single-point mutation. Also, the electrostatic complementarity remained evident at the interface, which indicated to us that binding was predicated on broad surface interactions rather than on individual residues, which ascertained Objective 3 and Objective 4.

Biological and Therapeutic implications: The interaction of LiGAPDH with C5a mirrors similar conserved strategies used by pathogens for evasion of the complement system by GAPDH sequestering C5a using charged surfaces. These results identify a targetable complementary electrostatic cavity as a potential broad-spectrum therapeutic target. Based on these findings, Objective 5 was achieved in establishing targetable therapeutic strategies that disrupt the interaction of LiGAPDH with C5a.

Final Synthesis: This study found that the complement evasion mechanism of LiGAPDH relies on cooperative electrostatic interactions rather than critical single residues. Thus, prioritizing developing therapies with this charged cavity as a target, providing groundwork development strategies to target other diseases such as leptospirosis, caused by *Leptospira*.

Bibliography

1) Fernández FJ, Gómez S, Vega MC. Pathogens' toolbox to manipulate human complement. Semin Cell Dev Biol. 2019 Jan;85:98-109. doi: 10.1016/j.semcdb.2017.12.001. Epub 2017 Dec 14. PMID: 29221973.
2) West EE, Kolev M, Kemper C. Complement and the Regulation of T Cell Responses. Annu Rev Immunol. 2018 Apr 26;36:309-338. doi: 10.1146/annurev-immunol-042617-053245. PMID: 29677470; PMCID: PMC7478175.
3) Guo RF, Ward PA. Role of C5a in inflammatory responses. Annu Rev Immunol. 2005;23:821-52. doi: 10.1146/annurev.immunol.23.021704.115835. PMID: 15771587.
4) Santos-López J, de la Paz K, Fernández FJ, Vega MC. Structural biology of complement receptors. Front Immunol. 2023 Sep 11;14:1239146. doi: 10.3389/fimmu.2023.1239146. PMID: 37753090; PMCID: PMC10518620.
5) Bharti AR, Nally JE, Ricaldi JN, Matthias MA, Diaz MM, Lovett MA, Levett PN, Gilman RH, Willig MR, Gotuzzo E, Vinetz JM; Peru-United States Leptospirosis Consortium. Leptospirosis: a zoonotic disease of global importance. Lancet Infect Dis. 2003 Dec;3(12):757-71. doi: 10.1016/s1473-3099(03)00830-2. PMID: 14652202.
6) Al Hariri YK, Sulaiman SAS, Khan AH, Adnan AS, Al-Ebrahem SQ. Determinants of prolonged hospitalization and mortality among leptospirosis patients attending tertiary care hospitals in northeastern state in peninsular Malaysia: A cross sectional retrospective analysis. Front Med (Lausanne). 2022 Sep 9;9:887292. doi: 10.3389/fmed.2022.887292. PMID: 36160172; PMCID: PMC9500579.
7) Picardeau M. Virulence of the zoonotic agent of leptospirosis: still terra incognita? Nat Rev Microbiol. 2017 May;15(5):297-307. doi: 10.1038/nrmicro.2017.5. Epub 2017 Mar 6. PMID: 28260786.
8) Pappas G, Cascio A. Optimal treatment of leptospirosis: queries and projections. Int J Antimicrob Agents. 2006 Dec;28(6):491-6. doi: 10.1016/j.ijantimicag.2006.08.021. Epub 2006 Nov 2. PMID: 17084067.
9) Navas-Yuste S, de la Paz K, Querol-García J, Gómez-Quevedo S, Rodríguez de Córdoba S, Fernández FJ, Vega MC. The structure of *Leptospira interrogans* GAPDH sheds light into an immunoevasion factor that can target the anaphylatoxin C5a of innate immunity. Front Immunol. 2023 Jun 20;14:1190943. doi: 10.3389/fimmu.2023.1190943. PMID: 37409124; PMCID: PMC10318897.
10) Laemmli UK. Cleavage of structural proteins during the assembly of the head of bacteriophage T4. Nature. 1970 Aug 15;227(5259):680-5. doi: 10.1038/227680a0. PMID: 5432063.
11) Jones G, Jindal A, Ghani U, Kotelnikov S, Egbert M, Hashemi N, Vajda S, Padhorny D, Kozakov D. Elucidation of protein function using computational docking and hotspot

analysis by ClusPro and FTMap. Acta Crystallogr D Struct Biol. 2022 Jun 1;78(Pt 6):690-697. doi: 10.1107/S2059798322002741. Epub 2022 May 25. PMID: 35647916; PMCID: PMC9159284.

12) Desta IT, Porter KA, Xia B, Kozakov D, Vajda S. Performance and Its Limits in Rigid Body Protein-Protein Docking. Structure. 2020 Sep 1;28(9):1071-1081.e3. doi: 10.1016/j.str.2020.06.006. Epub 2020 Jul 9. PMID: 32649857; PMCID: PMC7484347.
13) Vajda S, Yueh C, Beglov D, Bohnuud T, Mottarella SE, Xia B, Hall DR, Kozakov D. New additions to the ClusPro server motivated by CAPRI. Proteins. 2017 Mar;85(3):435-444. doi: 10.1002/prot.25219. Epub 2017 Jan 5. PMID: 27936493; PMCID: PMC5313348.
14) Kozakov D, Hall DR, Xia B, Porter KA, Padhorny D, Yueh C, Beglov D, Vajda S. The ClusPro web server for protein-protein docking. Nat Protoc. 2017 Feb;12(2):255-278. doi: 10.1038/nprot.2016.169. Epub 2017 Jan 12. PMID: 28079879; PMCID: PMC5540229.
15) Kozakov D, Beglov D, Bohnuud T, Mottarella SE, Xia B, Hall DR, Vajda S. How good is automated protein docking? Proteins. 2013 Dec;81(12):2159-66. doi: 10.1002/prot.24403. Epub 2013 Oct 17. PMID: 23996272; PMCID: PMC3934018.
16) Janson G, Paiardini A. PyMod 3: a complete suite for structural bioinformatics in PyMOL. Bioinformatics. 2021 Jun 16;37(10):1471-1472. doi: 10.1093/bioinformatics/btaa849. PMID: 33010156.
17) Kastritis PL, Bonvin AM. Are scoring functions in protein-protein docking ready to predict interactomes? Clues from a novel binding affinity benchmark. J Proteome Res. 2010 May 7;9(5):2216-25. doi: 10.1021/pr9009854. Erratum in: J Proteome Res. 2011 Feb 4;10(2):921-2. PMID: 20329755.
18) Dubendorff JW, Studier FW. Controlling basal expression in an inducible T7 expression system by blocking the target T7 promoter with lac repressor. J Mol Biol. 1991 May 5;219(1):45-59. doi: 10.1016/0022-2836(91)90856-2. PMID: 1902522.
19) Eriksson AE, Baase WA, Zhang XJ, Heinz DW, Blaber M, Baldwin EP, Matthews BW. Response of a protein structure to cavity-creating mutations and its relation to the hydrophobic effect. Science. 1992 Jan 10;255(5041):178-83. doi: 10.1126/science.1553543. PMID: 1553543.
20) Camilloni C, Sala BM, Sormanni P, Porcari R, Corazza A, De Rosa M, Zanini S, Barbiroli A, Esposito G, Bolognesi M, Bellotti V, Vendruscolo M, Ricagno S. Rational design of mutations that change the aggregation rate of a protein while maintaining its native structure and stability. Sci Rep. 2016 May 6;6:25559. doi: 10.1038/srep25559. PMID: 27150430; PMCID: PMC4858664.
21) Terao Y, Yamaguchi M, Hamada S, Kawabata S. Multifunctional glyceraldehyde-3-phosphate dehydrogenase of Streptococcus pyogenes is essential for evasion from neutrophils. J Biol Chem. 2006 May 19;281(20):14215-23. doi: 10.1074/jbc.M513408200.

Epub 2006 Mar 24. PMID: 16565520.

22) Querol-García J, Fernández FJ, Marin AV, Gómez S, Fullà D, Melchor-Tafur C, Franco-Hidalgo V, Albertí S, Juanhuix J, Rodríguez de Córdoba S, Regueiro JR, Vega MC. Crystal Structure of Glyceraldehyde-3-Phosphate Dehydrogenase from the Gram-Positive Bacterial Pathogen *A. vaginae*, an Immunoevasive Factor that Interacts with the Human C5a Anaphylatoxin. Front Microbiol. 2017 Apr 10;8:541. doi: 10.3389/fmicb.2017.00541. PMID: 28443070; PMCID: PMC5385343.

23) Gómez S, Querol-García J, Sánchez-Barrón G, Subias M, González-Alsina À, Franco-Hidalgo V, Albertí S, Rodríguez de Córdoba S, Fernández FJ, Vega MC. The Antimicrobials Anacardic Acid and Curcumin Are Not-Competitive Inhibitors of Gram-Positive Bacterial Pathogenic Glyceraldehyde-3-Phosphate Dehydrogenase by a Mechanism Unrelated to Human C5a Anaphylatoxin Binding. Front Microbiol. 2019 Feb 26;10:326. doi: 10.3389/fmicb.2019.00326. PMID: 30863383; PMCID: PMC6400076.

Annex

Annex 1: The following table lists the LiGAPDH residues predicted to be involved in the interaction with C5a, as identified by docking models. Residues are grouped by chain (Q and P) and shown with their position and amino acid type according to the UniProt sequence Q72QM3 (Q72QM3_LEPIC).

Chain Q	Chain P
Residues 75–81: Ser75, Glu76, Arg77, Asp78, Pro79, Glu80, Lys81	Residue 7: Asn7
Residues 183–185: Ala183, Thr184, Gln185	Residues 36–38: Thr36, Pro37, Asp38
Residues 192–196: Ser192, Lys193, Lys194, Asp195, Phe196	Residues 96–97: Thr96, Gly97
	Residues 182–186: Thr182, Ala183, Thr184, Gln185, Pro186
	Residues 191–196: Pro191, Ser192, Lys193, Lys194, Asp195, Phe196

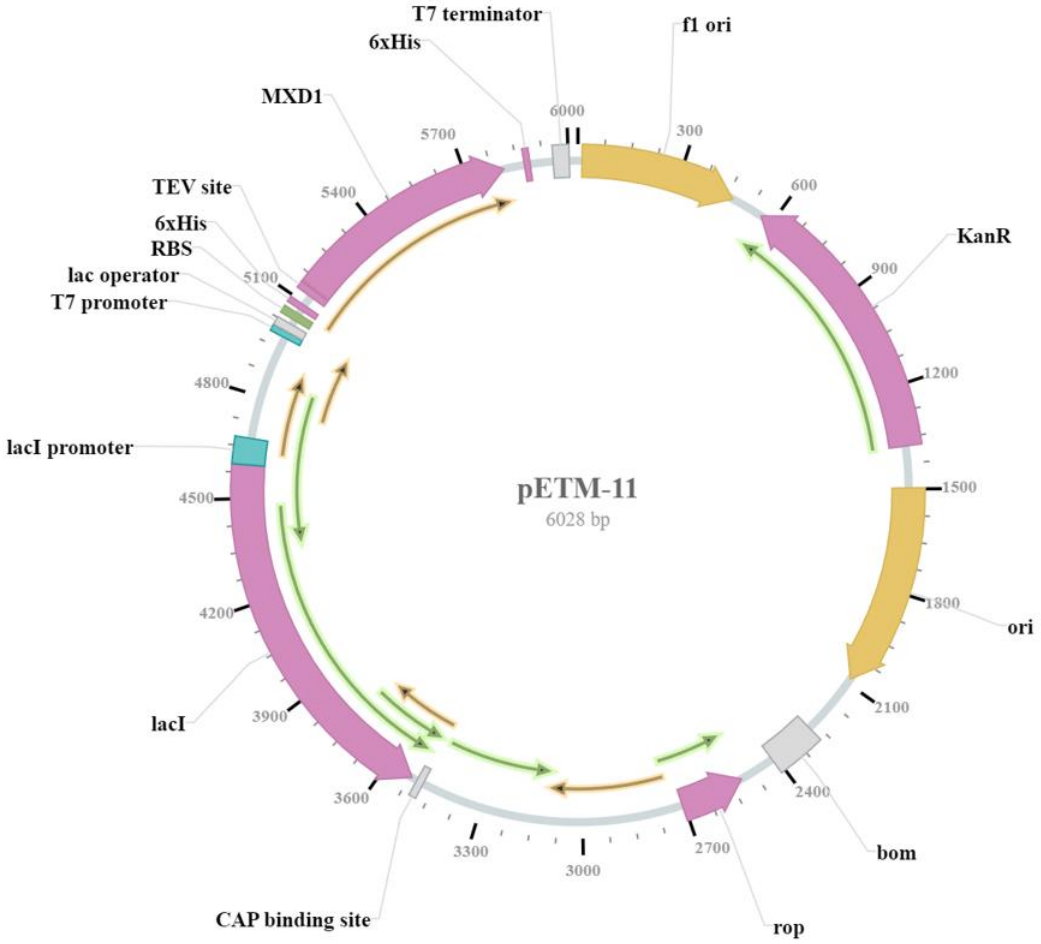

Annex 2: Map of the expression vector pETM-11. Image adapted from the Addgene plasmid database (Addgene: pETM11-ACS).

A WT

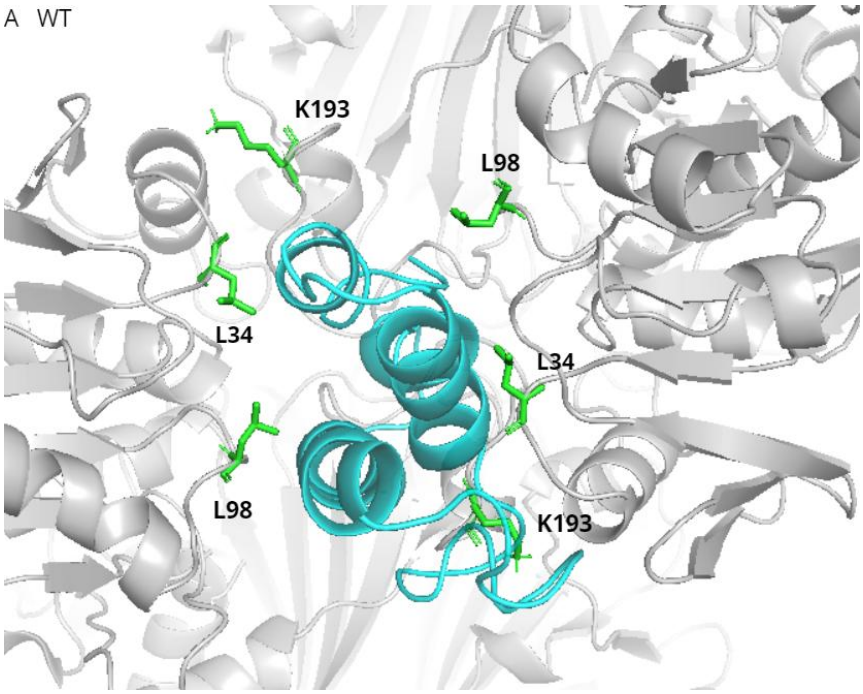

B L34A

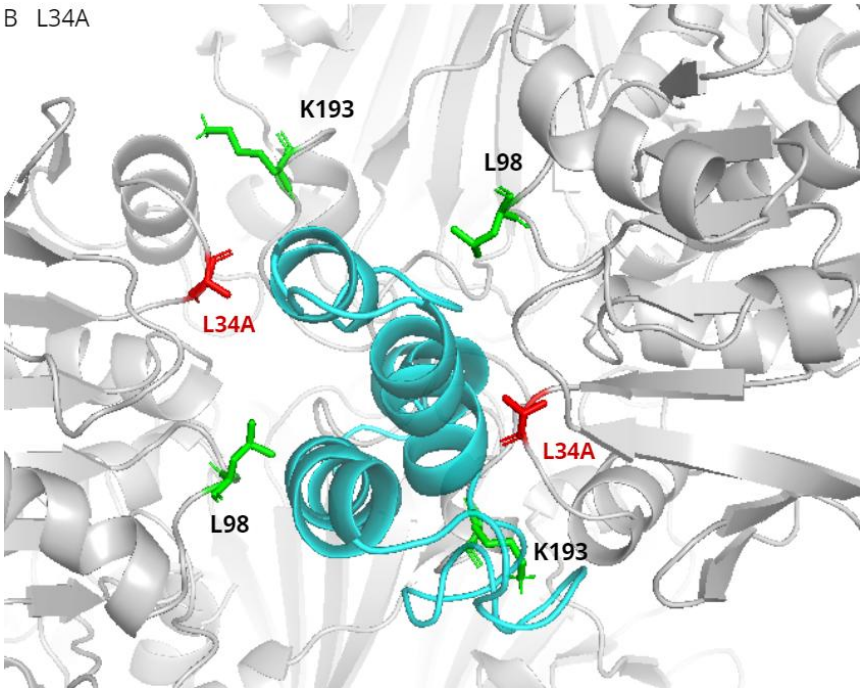

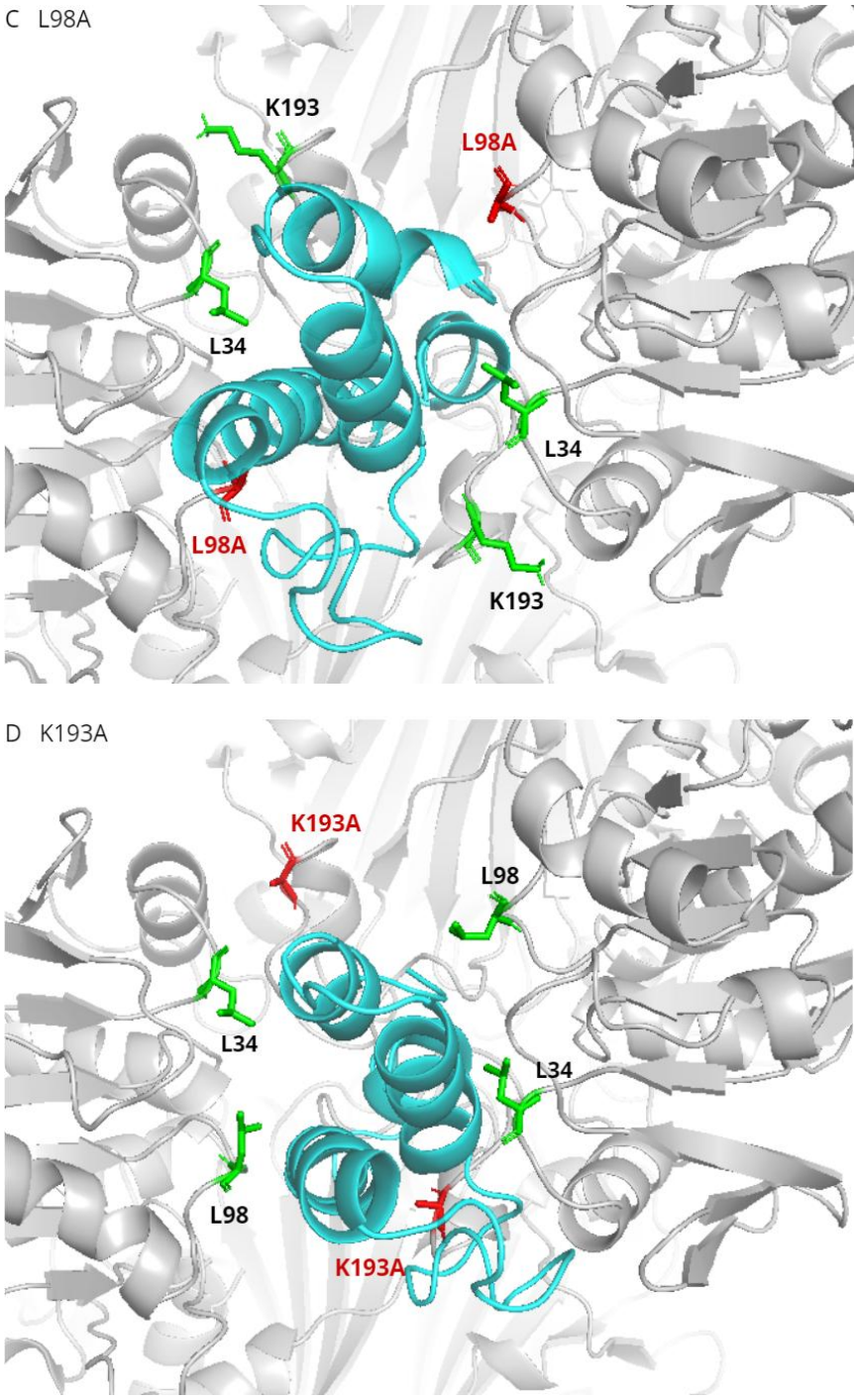

Annex 3. Docking models of the interaction between LiGAPDH and C5a. The structures of LiGAPDH (PDB: 8OHA) and C5a (PDB: 1KJS) were used as starting templates. The LiGAPDH mutants L34A, L98A, and K193A were generated in silico using the PyMOL mutagenesis tool prior to docking, and the corresponding interaction models were then obtained using ClusPro and visualized in PyMOL. In all panels, C5a is shown as a cyan cartoon. LiGAPDH residues located within 4 Å of C5a, potentially involved in the interaction, are highlighted. LiGAPDH is represented in grey. The non-mutated residues analyzed in this study (L34, L98, K193) are displayed as green sticks and labeled, while the mutated residues are shown in red. All panels are displayed in the same orientation. (A) Wild-type complex. (B) CVC0189 L34A mutant. (C) CVC0190 L98A mutant. (D) CVC0191 K193A mutant.

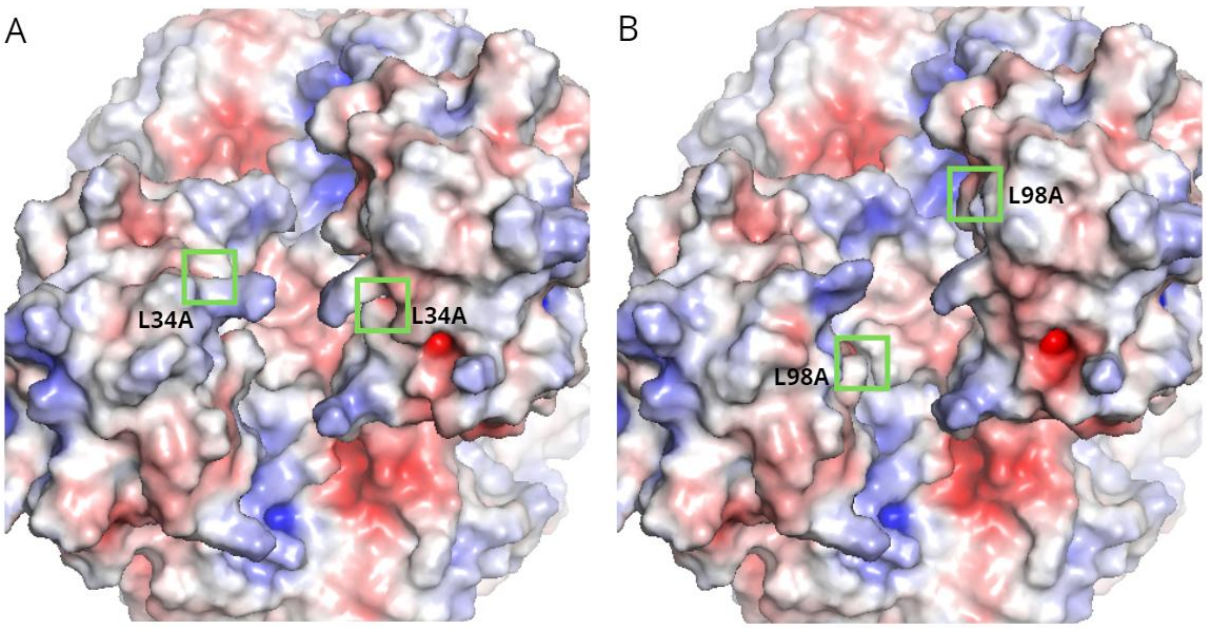

Annex 4: Electrostatic potential surface representations of LiGAPDH single-point mutants (L34A and L98A), generated in PyMOL. The structure (PDB: 8OHA) was used as a template, and both mutants were constructed in silico using the PyMOL mutagenesis tool. (A): Electrostatic potential of the L34A mutant. (B): Electrostatic potential of the L98A mutant.

ANEXO IX

Título del Trabajo: Site-Directed Mutagenesis and Structural Modeling of the LiGAPDH–C5a Interface in Immune Evasion/ Mutagénesis dirigida y modelado estructural de la interfaz LiGAPDH–C5a en la inmunoevasión.

Este trabajo ha sido realizado en el Grupo de

Structural Biology of Host-Pathogen Interactions of CIB MS – CSIC

Tutor/es: Sara Gómez Quevedo (Universidad Europea de Madrid, Facultad de Ciencias Biomédicas, Departamento de Biociencias) y María Cristina Vega Fernández (Centro de investigaciones Biológicas Margarita Salas- Consejo Superior de Investigaciones Científicas)